Adsorption of volatile organic compounds by ZIF-8, Cu-BTC and a Prussian blue analogue: A comparative study

Lotfi Boudjema, Jérome Long, Hugo Petitjean, Joulia Larionova, Yannick Guari, Philippe Trens, Fabrice Salles

Adsorption of Volatile Organic Compounds by ZIF-8, Cu-BTC and a Prussian blue analogue: A comparative study

Lotfi Boudjema, Jérôme Long, Hugo Petitjean, Joulia Larionova, Yannick Guari, Philippe Trens* and Fabrice Salles*

Institut Charles Gerhardt Montpellier, UMR 5253, Université de Montpellier, CNRS, ENSCM, 240 avenue du Professeur Émile Jeanbrau and Place E. Bataillon, 34296 Montpellier Cedex 5, France.

Emails : fabrice.salles@umontpellier.fr; philippe.trens@enscm.fr

Keywords : Cu-BTC; ZIF-8; Prussian blue analogue; sorption; hydrostability

Abstract.

In this paper, a Prussian blue analogue $Co[Co^{III}(CN)_6]_{0.66}\cdot 5.2H_2O$ and commercial Cu-BTC and ZIF-8 materials are compared in terms of their sorption capabilities for water or hydrocarbons. Experimental and theoretical approaches were combined in order to better understand the microscopic mechanisms ruling their different sorption properties. It was first demonstrated that amongst the three materials investigated, ZIF-8 was the most hydrophobic, whereas the PBA was more hydrophilic. In terms of sorption capacities, Cu-BTC is highly efficient for adsorption of the investigated hydrocarbons with large adsorption capacities (150 $mg.g^{-1}$), however, it has proven unstable in the presence of water and cannot be used for humid hydrocarbons adsorption and separation. *n*-Hexane is preferentially adsorbed (250 $mg.g^{-1}$ at saturation) in the hydrophobic ZIF-8, whereas cyclohexene is not, due to the size of the windows. Even if ZIF-8 did not adsorb water, its porosity decreased in the presence of water. On the contrary, CoCo is stable in humid conditions and even if its sorption capacity is

lower than that found for the other MOFs investigated, it seems more appropriate for humid hydrocarbons sorption or separation.

1. Introduction

In industrial gas treatment processes, the currently used benchmark adsorbents are activated carbons, zeolites, silicas or alumina.[1] However, many of them present several drawbacks usually associated with their low efficiency in humid conditions, the high cost of their regeneration and the low diffusivity of gas species. The main problem is related to the presence of water vapour in the gas stream making the separation or adsorption of Volatile Organic Compounds (VOCs) very difficult and rapidly ineffective. Water due to its polarity, is frequently in competition with organic vapours for the active sites and for this reason it is often considered as a poison for the adsorbents.[2] Depending on the application, saturated adsorbents are either eliminated (portable applications, such as gas masks) or regularly regenerated (static applications, such as plants).[1,3] To circumvent this problem in industrial processes, water is generally removed beforehand from the hydrocarbons streams using alumina columns, which requires an introduction of an additional step and then rises the cost of the overall procedure.[4,5] For this reason, alternative adsorbent materials able to efficiently adsorb VOCs in humid conditions are extremely challenging.

On the other hand, in some cases, water can enhance the adsorption capacity of porous materials. For instance, such effect has been demonstrated for xylene separation on Ba^{2+} exchanged faujasite, [6] for CO_2 capture in Al-MIL-53 [7] or for ammonia adsorption by activated carbons.[8] As a consequence, the hydrophilic-hydrophobic balance of the adsorbent is a key feature, which will determine the impact of separation/adsorption in humid conditions, either at traces or at high concentrations and therefore the efficiency of the adsorbent.[9] If the hydrophilic-hydrophobic feature for simple surface characterisation is a

relatively well understood process, this phenomenon is much more complex in the case of porous solids due to the additional dimension brought by porosity, as well as the interplay between the surface chemistry and confinement effects. Moreover, reported works on this subject are relatively scarce [10,11], but they highlight the important role of the hydrophilic / lipophilic balance for the separation of hydrocarbons.[11]

Molecular chemistry represents an appealing synthetic strategy of choice to design optimized molecule-based materials with large internal surface areas, high porosity and an excellent chemical selectivity, which may be considered as promising adsorbents for gas separation applications.[12,13] These materials exhibit many advantages, such as soft chemistry routes, light density, optical transparency, high degree of structural diversity and tunability in comparison with their mineral oxides counterparts. Furthermore, due to their chemical and structural flexibility and the possibility of post-synthetic modifications, the hydrophilic/hydrophobic balance and therefore the adsorption of gases or vapours in humid conditions could be finely tuned depending on the targeted applications.[13–15] Among these, two families of molecule-based materials have been extensively investigated in the scope the gas separation: Metal-Organic Frameworks (MOFs) and porous cyano-bridged coordination polymers called Prussian Blue Analogous (PBA).[14,16–18]

MOFs materials have been widely investigated for adsorption of different gas and species, [19–22] but only a few works may be cited on the investigation of their hydrophilic/ hydrophobic behavior and hydrostability.[17] Moreover, there are no detailed studies on their materials efficiency and precise description of the separation/adsorption processes in the presence of water and particularly on the competitive adsorption. [14,16,18,22] As concern PBAs, despite a relatively high thermal stability and the important structural and chemical robustness of these materials, much less investigations have generally been done on their use for gas separation and for hydrocarbon or VOCs adsorption. [7,23,24]

Recently, we reported on the synthesis of a series of highly performant porous PBA materials, their hydrostability and their ability to efficiently separate different vapors, such as water, *n*-pentane, *n*-hexane, cyclohexane and cyclohexene.[11] In particular, the $Co[Co^{III}(CN)_6]_{0.66}\cdot 5.2H_2O$ PBA (denoted in the following text as CoCo) exhibits strong hydrothermal stability up to 300 °C and an interesting ability to switch its hydrophobic and hydrophilic character as a function of the saturation of the metal centers, allowing the efficient separation of hydrocarbons in a dry and humid atmosphere.[25] In this article we report further investigations on the microscopic adsorption mechanisms occurring in CoCo during water or hydrocarbons adsorption by using the combination of experimental means and theoretical modeling and compare its performance with two reference MOFs materials (commercial ZIF-8 and Cu-BTC). A particular emphasis is given here on the understanding of the selected VOCs' adsorption mechanisms both, in dry and in humid conditions through adsorption measurements combined with Monte Carlo simulations considering adsorption and VOCs-water co-adsorption and comparison of hydrostability of host frameworks.

2. Experimental section

2.1. Materials. Hydrocarbons (*n*-pentane, *n*-hexane, cyclohexane, cyclohexene) were provided by Aldrich (purity above 99%) and stored over activated 3A molecular sieve. These were outgassed at low pressure before use. Water was deionized and outgassed at low pressure before being used as sorbate.

ZIF-8 (2-methylimidazole zinc salt, $C_8H_{10}N_4Zn$) and Cu-BTC (copper benzene-1,3,5-tricarboxylate, $C_{18}H_6Cu_3O_{12}$) were provided by Aldrich and used without any purification. They were activated at 250°C for 8h before sorption studies. $Co[Co^{III}(CN)_6]_{0.66}\cdot 5.2H_2O$ (CoCo) was prepared following the well-defined procedure by the self-assembly reaction between $[Co^{III}(CN)_6]^{3-}$ and $[Co(H_2O)_6]^{2+}$ in water. In details, a solution of $K_3[Co(CN)_6]$ (10 mmol) in 100 mL of ultrapure water was added dropwise to a solution of $Co(NO_3)_2\cdot 6H_2O$ (18

mmol) in 100 mL of ultrapure water. The immediately formed precipitate was stirred overnight. The obtained solid was then centrifuged, washed with ultrapure water and dried in air. The powdered CoCo, as well as Cu-BTC and ZIF-8 were further characterized for determining their structural and textural properties before performing separation experiments.

2.2. Methods. CHN elemental analyses were performed on CoCo. The composition of the calcined PBA was found to be: % C: 16.04 (16.06), % H: 3.03 (3.51); % N: 18.94 (18.91). Thermogravimetric analyses were obtained for the three materials with a thermal analyzer STA 409 Luxx® (Netzsch) on the range 25 – 1000 °C at heating speed of 2 °C /min. Two main pieces of information could be deduced: (*i*) the thermal stability of the materials, and (*ii*) the water content of PBA allowing for the full determination of the structure of PBA. The exact formulas of PBAs could be deduced, taking into account the water loss at 150 °C obtained by TGA analysis (see Figure 1 and Table 1). The vapour sorption experiments were performed with a set-up developed in our laboratory.[26,27] The adsorbed amounts could be determined by the equilibrium pressure difference before and after adsorption steps. For reaching the appropriate accuracy, two capacitive pressure gauges of 10 Torr and 1000 Torr were used. The tested materials were activated *in situ* at 200 °C under secondary vacuum. The adsorption device described in Refs [26,27] is driven by the choice of the initial pressure, that is before the sorbate is contacted with the sorbent (rather than the equilibrium pressure). The thermal stability during the measurements was better than 0.10 K. Sorption experiments were performed at 303 or 313 K. To avoid any condensation in the apparatus, the maximum relative pressure was chose at 0.9. Nitrogen adsorption experiments were conducted before and after chromatographic separation in order to evaluate the textural properties of the materials on duty and therefore their hydrostability. The adsorption isotherms of nitrogen were determined at 77 K by using a Micromeritics ASAP 2020 surface area analyzer. All materials analyzed were treated thermally under nitrogen at 250 ^{o}C for 8 h before

measurements were started. The BET model was applied in the relative pressure range 0.05-0.20 for determining the equivalent specific surface areas of the microporous materials. The cross-sectional area of the nitrogen molecule was taken as 0.162 nm^2.

Scanning Electronic Microscopy analyses (SEM) were performed on a FEI Quanta FEG 200 instrument. The powders were deposited on an adhesive carbon film and analyzed under vacuum. The quantification of the heavy elements was carried out with the INCA software, with a dwell time of 3 µs.

X-ray powder diffraction patterns were recorded at room temperature with the XPERTPro analytical diffractometer mounted in a Debye−Scherrer configuration and equipped with a $Cu_{k\alpha}$ radiation (λ = 1.5418 Å).

2.3. Computational section

2.3.1. Modeling of structures

The structures for the molecular simulations for CoCo, ZIF-8 and Cu-BTC are issued from the literature [25] and reported in Figure 1.

In the case of co-adsorption in presence of water for PBA, a structure containing cobalt metal centers saturated with water molecules to model the chemisorbed H_2O species was also considered in CoCo sample, as already presented in the literature. Indeed it has already been proved that the water molecules chemically bonded to the unsaturated metal center strongly modify the affinity of the solid for water and therefore for alkanes/alkenes.[25]

2.3.2. Textural Properties

Starting from these structures, it is then possible to determine both, the specific surface area accessible for the nitrogen molecule and the pore free volume. The accessible surface area was calculated using the strategy previously developed by Düren et al.[28] For this, the center of a nitrogen probe molecule (with a diameter equal to 3.681 Å) is rolling across the surface.

The diameters of each atom constituting the investigated structures were taken from the Universal force field (UFF).[29] The free volume was also calculated for each simulated structure by a trial insertions method with a probe size equal to 0 Å within the entire volume of the unit cell. This calculation enables us to determine the volume of the unit cell unoccupied by the atoms of the framework and compared to the free volume deduced from experimental nitrogen sorption isotherms. Using the same parameters for the framework (UFF), the methodology of Gelb and Gubbins was used to calculate the pore size distribution.[30] Such approaches have successfully been used in ZIFs and other MOFs.[31,32]

2.3.3. Monte Carlo Simulations

Using the previous structural models, classical Grand Canonical Monte Carlo (GCMC) [33] simulations have been performed to calculate the adsorption isotherm for the different vapors investigated here and Monte Carlo at low loadings (1 molecule/ unit cell) to estimate the adsorption enthalpy at low coverage. GCMC simulations were performed by means of the home-made code with typically 20 x 10^6 Monte Carlo steps for equilibration and 5 x 10^6 steps for production for alkane vapors. In contrast, the water behavior in the solids was investigated using 100 x 10^6 steps for equilibration and 20 x 10^6 steps for production. The electrostatic contribution was calculated using the Ewald summation while the short-range interactions were computed with a cut-off distance of 12 Å. The simulations were conducted at 303 K. The structures are considered as rigid: it means that the cell parameters are fixed and multi-cells are considered to allow us to use a cut-off distance of 12 Å.

Regarding the determination of the adsorption enthalpy, similar number of steps was considered. Supplementary calculations were also performed in order to estimate the co-adsorption properties for linear alkane and water or cyclic compound and water couples. For

that purpose, different compositions water-alkane (by restricting to n-hexane) or water-alkene (by restricting to cyclohexene) have been tested in order to compare with experimental data. We have chosen 10-90, 50-50 and 30-70 ratios in simulations. It was therefore possible to distinguish the different molecules arrangements and elucidate the distribution of the adsorbed molecules in co-adsorption.

2.3.4. Force Fields

UFF force field for the atoms of the framework and partial charges evaluated from the electronegativity equalization method implemented in Material Studio have been used for the solids.[34] In the case of the vapors, TIP4P-2005 and TraPPE have been implemented in the code for water and alkanes hexane and cyclohexene) respectively.[35–37]. Such a combination of the force fields has already proved to be efficient for the prediction of the adsorption of gases and vapors occurring in MOF materials. [38,39] Additionally, a force field has also been tested for cyclohexene considering DFT partial charges (see Figure S1) and UFF parameters. In this case, DFT calculations have been performed to calculate partial charges after geometry optimization of the molecule using the PW91 GGA density functional and the double numerical basis set containing polarization functions on hydrogen atoms (DNP) as implemented in $DMol^3$ code. [40] The adsorbate/adsorbent Lennard-Jones interatomic potential parameters were then calculated using Lorentz Berthelot mixing rules.

When water is involved, calculations were performed on both, the CoCo structure containing water bonded to the unsaturated cobalt centers and the CoCo structure without water. The partial charges of the different structures considered are issued from the literature.[25]

3. Results and Discussion

3.1. Crystal structures and characterizations

ZIF-8 and Cu-BTC are commercially available MOFs. They were used as received after activation. The PBA material, $Co[Co^{III}(CN)_6]_{0.66}$ (CoCo) has been synthesized by using the well known procedure involving the self-assembly reaction between the hexacyanometallate precursor $[Co(CN)_6]^{3-}$ and $[Co(H_2O)_6]^{2+}$. The identity of the investigated materials has been confirmed by Infra-Red (IR) spectroscopy (Figure S2) and Powder X-Ray diffraction (PXRD) analysis (Figure S3).

The crystal structures for ZIF-8 and Cu-BTC from the literature [41]**,** as well as the adapted through molecular modeling structure for $Co[Co^{III}(CN)_6]_{0.66}$ are shown in Figure 1.[25] Note that the simulated PXRD patterns are in agreement with the experimental ones (Figure S3). The space groups, as well as the cell parameters for the investigated materials are summarized in Table SI1. Using these structural models, it is therefore possible to describe the textural properties and in particular the pore networks available in these different solids. All the pore radius and windows radius values are described from calculations of the pore size distribution for the structures investigated in this article (see Figure S4). The Cu-BTC structure (Figure 1a) corresponding to the $[Cu_3(btc)_2]$ (with btc= 1,3,5-benzenetricarboxylate) contains three distinct cages: one small octahedral cage (with a pore windows equal to 2.0 Å and a pore radius close to 5.2 Å) and another larger cuboctahedral cage with pore radius of 6.1 Å and connected by a window with a pore aperture radius equal to 2.6 Å. The ZIF-8 $[Zn\text{-}(MeIM)_2]$ (where MeIM= 2-methylimidazolate) cages (Figure 1b), has a structure containing zinc (Zn) atom interconnected with 2-methylimidazolate ligands and forming a sodalite topology with large cavities (11.4 Å) and small pore aperture (3.4 Å). Regarding the CoCo, the cubic face centered cubic network made by the coordination of hexacyanocobaltate moieties to Co^{2+} ions in the three space directions, different channels can be defined as a function of the presence of $[Co(CN)_6]^{3-}$ vacancies giving rise to the pore size radii close to 1.9 and 3.7 Å which corresponds to diameters of 3.8 Å and 7.4 Å respectively.

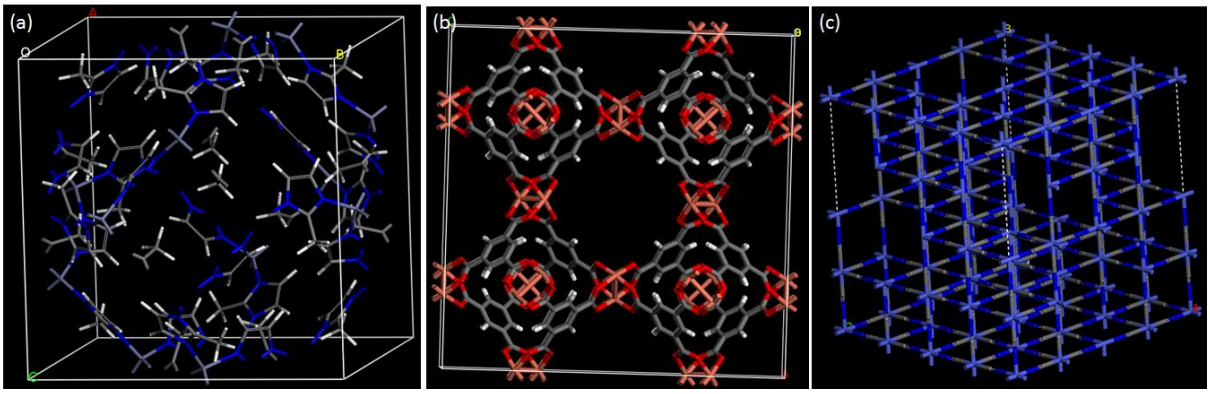

Figure 1. Crystallographic structures of ZIF-8 cages (Figure 1a), Cu-BTC structure (Figure 1b) and $Co[Co^{III}(CN)_6]_{0.66}$ (CoCo) (Figure 1c) obtained by modeling from the literature.

To confirm the description of the microscopic structures, the N_2 adsorption isotherms of Cu-BTC and ZIF-8 (Figure S5) are consistent with published results.[42,43] These adsorption isotherms are typical of microporous materials and are in agreement with the structure of these materials, in terms of windows sizes or cavities diameters.[44,45] The saturation plateaus are very flat, strongly suggesting that these materials are made of large microporous particles for which the external surface is negligible. In the case of CoCo, the adsorption isotherms are reminiscent of two populations of pores differing in size, probably due to the presence of pores created by double or multiple vacancies.[11] The main population is made of micropores, whereas a population of mesopores is also present. The microporosity can be readily deduced from the structure of these material which have channels of ~0.5 nm width, as confirmed by Figure S4 reporting the pore size distribution for the three solids. The mesoporosity can be deduced from the clear uptake of the adsorbed amount at $p/p° > 0.8$ followed by a saturation plateau, which indicates that mesoporosity is filled. Since the structure of CoCo does not reveal any mesoporous channels or cavities, this mesoporosity should be generated either by the distribution of the vacancies in CoCo, which would enlarge the original microporosity (double vacancies for instance) or by the intergranular voids. The

adsorption capacities of the materials have been compared at $p/p° = 0.5$, a relative pressure for which all adsorption isotherms are flat (see Figure S5). In terms of capacities, ZIF-8 and Cu-BTC are unsurprisingly the best materials studied whereas CoCo appears less appealing in terms of textural properties.

The thermal stability of ZIF-8 and Cu-BTC materials was checked by thermogravimetric analysis and the thermal stability of CoCo which has been previously investigated was added for comparison in Figure S6.[11] Concerning Cu-BTC and CoCo, two main weight losses can be distinguished: the first step occurs up to 150 °C, which can be classically attributed to the desorption of physically adsorbed water, while the second step at higher temperature (at around 300 °C) corresponds to the material's decomposition. In the case of ZIF-8, the weight loss occurs at a higher temperature (450 °C), indicative of the higher thermal stability. As compared to the other materials, there is no loss at low temperature usually attributed to water removal, confirming the hydrophobic character of ZIF-8. The degradation of ZIF-8 happens in a main step indicative of the collapse of the structure and its full oxidation, as already observed in the literature. [46] The decomposition temperatures for all materials are reported in Table S1. Below 300 °C, all of them are thermostable,[47,48] and for these reasons, the activation stages for the adsorption experiments have been performed by heating at 200 °C during 12 h under a secondary vacuum to ensure the material's integrity.

It must be emphasized that all materials are thermostable at a relatively high temperature under static air, that makes them suitable for various applications including heterogeneous catalysis or chromatography.[49,50] However, the presence of water in the vapor mixtures could strongly impact their thermostability. This is why it is necessary to determine the thermodynamic performances of the material for adsorption of vapours in humid conditions. However, in a first step, the efficiency and the microscopic mechanisms for adsorption of dry vapours is studied.

3.2. Adsorption of dry vapours by Cu-BTC, ZIF-8 and CoCo

The comparison between experimental and theoretical adsorption isotherms for water and selected hydrocarbons (hexane and cyclohexene) on the different materials shown in Figure 2 and their adsorption capacities at $p/p°$ = 0.5, a relative pressure for which all adsorption isotherms are flat, are summarized in Table 1.

Table 1. Values of the amounts adsorbed (Qads in $mg.g^{-1}$) for hexane, cyclohexene, and water from the experimental and simulated isotherms determined in ZIF-8, Cu-BTC, and CoCo at $p/p° = 0.5$

		ZIF-8	**Cu-BTC**	**CoCo**
Hexane	Experimental	250	175	190
	Simulated	200	380	80
Cyclohexene	Experimental	20	150	195
	Simulated	250	550	110
Water	Experimental	0	0	375
	Simulated	0	0	180 / 0

The comparison between simulated and experimental adsorption isotherms shows a very good agreement for hexane in ZIF-8 (in particular for the saturation capacity Qads = 250 $mg.g^{-1}$ and 200 $mg.g^{-1}$ from the experimental and simulated isotherms), illustrating that the force fields considered in these calculations are consistent. In contrast, in the case of Cu-BTC, the theoretical adsorption is much larger than the experimental one (Qads at $p/p° = 0.5$ is equal to 380 $mg.g^{-1}$ compared to the simulated values at 175 $mg.g^{-1}$), which can be explained by the inaccessibility of some pores or their blocking by the hexane molecules in ball-shaped conformation. In the case of CoCo, experimental (190 $mg.g^{-1}$) Qads values are higher than the

simulated ones (80 $mg.g^{-1}$), which could be explained by the absence in the modeled structures of pores formed by the double vacancies or by a large amount adsorbed on the external surface.

Regarding the cyclohexene, a relative good agreement is obtained for CoCo, but the actual amounts adsorbed in Cu-BTC and ZIF-8 are lower than the theoretical values certainly due to some pores inaccessibility. Indeed when we compare the size of the cyclohexene (5.2 x 4.4 x 3.1 Å) with pore aperture in ZIF-8 (3.4 Å) and pore size in Cu-BTC (5.2 Å), it appears that the molecule has dimensions very close to the apertures allowing it to enter in the cavity, which is not taken in considerations with the Monte Carlo calculations. In the case of ZIF-8, it can be noted that there is almost no adsorbed cyclohexene experimentally. Such behavior could be explained by the size of the network's windows, which is smaller than the size of the considered molecule, and thus avoid the access to porosity. Note that different behavior of solids relative to the adsorption of hexane and cyclohexene will be explained later.

In the case of water, it is observed experimentally that the Cu-BTC is not stable under humid conditions and that the structure is destroyed upon adsorption isotherm measurements. In the case of ZIF-8, the experiments confirm that the solid is hydrophobic, which is in very good agreement with theoretical results giving the Qads value equal to values close to 0 $mg.g^{-1}$. CoCo displays a different behavior due to the chemisorption of water on the unsaturated metal centers upon water adsorption. Such behavior is confirmed by the comparison between the adsorption isotherms calculations in anhydrous and water-saturated CoCo structures. The switching between hydrophobic and hydrophilic characters of the CoCo has already been discussed in the literature. The difference between dehydrated and hydrated structures is mainly based on the partial charges on the atoms due to the presence of chemisorbed water. This leads to modify the hydrophilicity/hydrophobicity character of the solid as a function of the chemisorbed water amount. We have already proved that dehydrated CoCo (mainly

hydrophobic) does not adsorb any water molecules while CoCo containing chemisorbed water can adsorb easily physisorbed water molecules at very low pressures (which means that the solid is hydrophilic in these conditions). Such a behaviour has already been evidenced in Boudjema et al. [25] Keep in mind that the amount of adsorbed water reported in the theoretical adsorption isotherms report only physisorbed water.

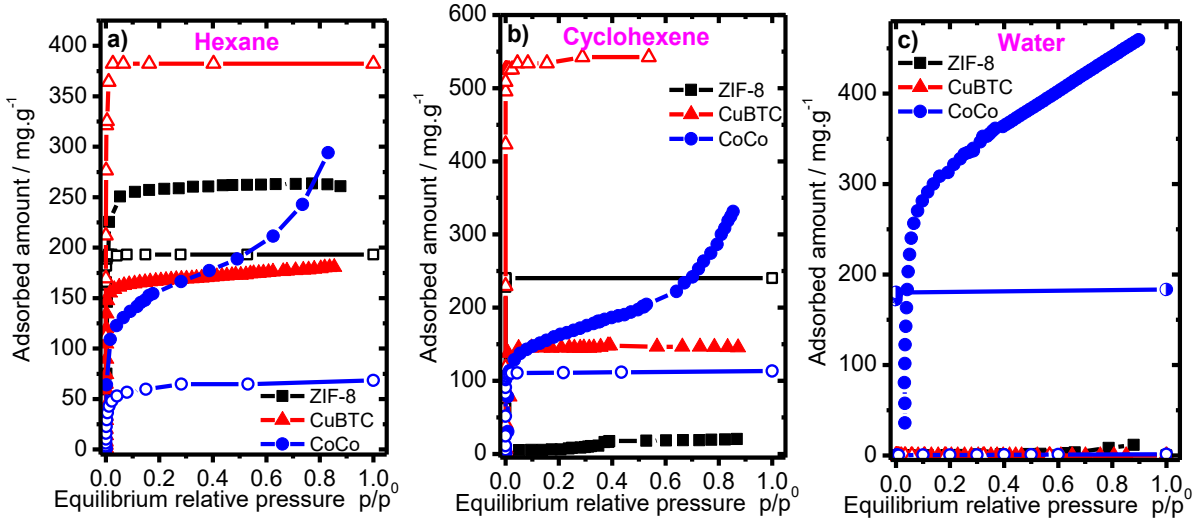

Figure 2. Experimental measured at 303 K (filled symbols) and simulated (open symbols) adsorption isotherms of selected vapours (hexane (a), cyclohexene (b) and water c) for CoCo (blue circles); Cu-BTC (red triangles), and ZIF-8 (black squares). For c), the half-filled symbols corresponds to the simulated isotherms with hydrated CoCo.

The enthalpies of adsorption at low coverage extracted from modeling are given in Table 2.

Table 2. Enthalpies of adsorption (kJ.mol^{-1}) in the three solids at low coverage (1 molecule per cell) from Monte Carlo calculations. A comparison can be made with the enthalpies of liquefaction at 313 K of the different sorbates (last row). In the case of the hydrated CoCo material, the theoretical adsorption enthalpy is -40 kJ.mol^{-1}.[25]

ΔH / kJ.mol^{-1}	Water	*n*-Hexane	Cyclohexene
Cu-BTC	-24	-68	-88

ZIF-8	-15	-56	-58
Dehydrated CoCo	-16	-48	-54
$\Delta_{liq}H$	-44	-31	-32

In the case of adsorption enthalpy obtained by molecular simulations, a great affinity can be observed for linear and cyclic alkanes in the three investigated solids in this article. The following sequence based on the sorption enthalpy can be determined as: Cu-BTC > ZIF-8 > CoCo. This sequence is in good agreement with that obtained in the case of the adsorption isotherms. In contrast, the affinity of these solids for water seems to be similar and relatively weak: all the solids are hydrophobic after activation at 250°C. Keep in mind that the adsorption enthalpy at low loading for CoCo has been calculated for dehydrated structure (without chemisorbed water) and the results are different in presence of chemisorbed water molecules present in the structure since the structure becomes hydrophilic in this case.

The comparison is not so simple in the case of the different materials, since structural and textural properties as well as calculations defaults can be invoked to explain differences. The behavior of CoCo has already been discussed in a previous article showing the hydrophobic-hydrophilic switching in this material due to the chemisorbed water molecules fixed on the unsaturated Co metal centers.[25] However we have also to keep in mind that Monte Carlo simulations are not able to take into account the chemical interaction (chemisorption) occurring between the metal center and the first water molecules which can thereafter play the role of adsorption sites for the next water molecules. Indeed it would be required to use reactive force fields to be able to take into account the creation of covalent bonds between the metal center and the chemisorbed water molecules. It follows that the present calculations fail therefore to reproduce the energy release observed during the sorption of the water molecules on the unsaturated metal centers and the formation of a strong chemical bond.

Using molecular simulations, it was possible to analyze the distribution for hexane and cyclohexene in the different solids (see Figure 3) as well as the interactions of these molecules with the host frameworks in order to provide explanations of their different behaviors related to adsorption of these probe vapors. Since water molecules did not enter in ZIF-8 and Cu-BTC (hydrophobic characters), we did not focus on behavior of this sorbate.

However, and in the case of CoCo, the comparison between linear alkane and cyclohexene shows that the main localizations of the molecules are in the cavities resulting of the missing hexacyanocobaltate $[Co(CN)_6]^{3-}$. Furthermore, due to the linear geometry of the *n*-hexane, these later can visit the smaller pores, while the much larger cyclohexene moieties, cannot enter inside these pores.

In the case of Cu-BTC, the larger cavities are accessible to the both molecules investigated here, while the smaller cavities are only accessible in Monte Carlo simulations to the cyclohexene molecules, probably due to the stronger interactions between benzene rings, as confirmed by the illustrations of the main interaction sites (Figure 4). Keep in mind however that these small cavities should not be accessible due to the smaller aperture compared to the size of cyclohexene.

In the case of ZIF-8, similar adsorption behaviors seem to be observed regarding the distribution of the adsorbed molecules for both cyclohexene and *n*-hexane.

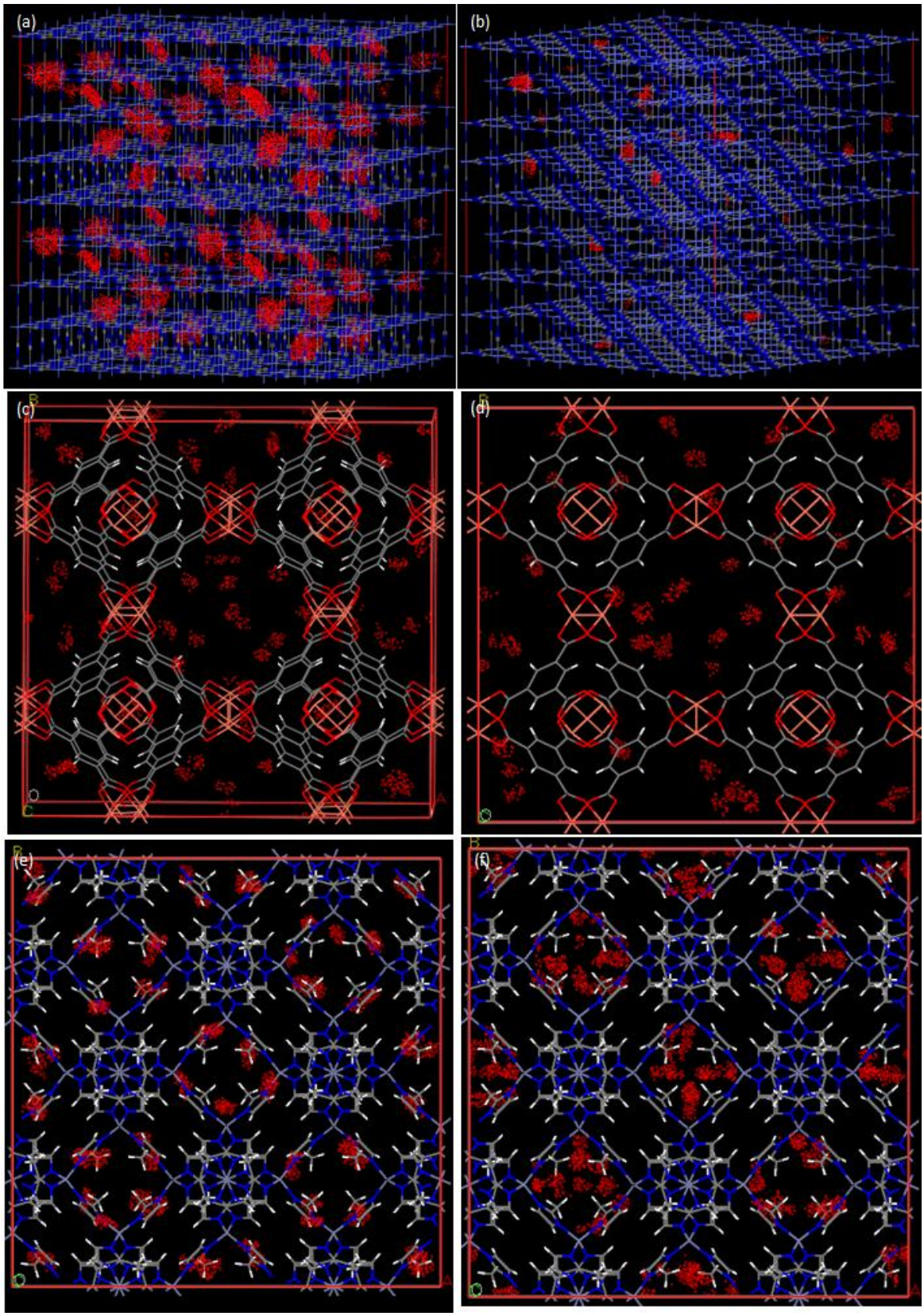

Figure 3. Distribution of hexane and cyclohexene molecules in CoCo ((a) and (b) respectively), Cu-BTC ((c) and (d) respectively) and ZIF-8 ((e) and (f) respectively)

By focusing on the main interactions sites (see Figure 4), it is possible to observe that the *n*-hexane and cyclohexene molecules did not interact with the same parts of the solid frameworks or with the same strength. Indeed, in the case of Cu-BTC, cyclohexene interacts more strongly with the benzene rings of the frameworks than the *n*-hexane molecules (distances between 2.5-2.8 Å for cyclohexene and 3.2-3.5Å for *n*-hexane). We observed a similar behavior in the case of ZIF-8 but, in this case, the both molecules interact with a similar strength with the benzene ring of the framework (3.3-3.5 Å for hexane and 3.0-3.3 Å for cyclohexene), which can account for the similar adsorption enthalpy at low coverage obtained from Monte Carlo simulations.

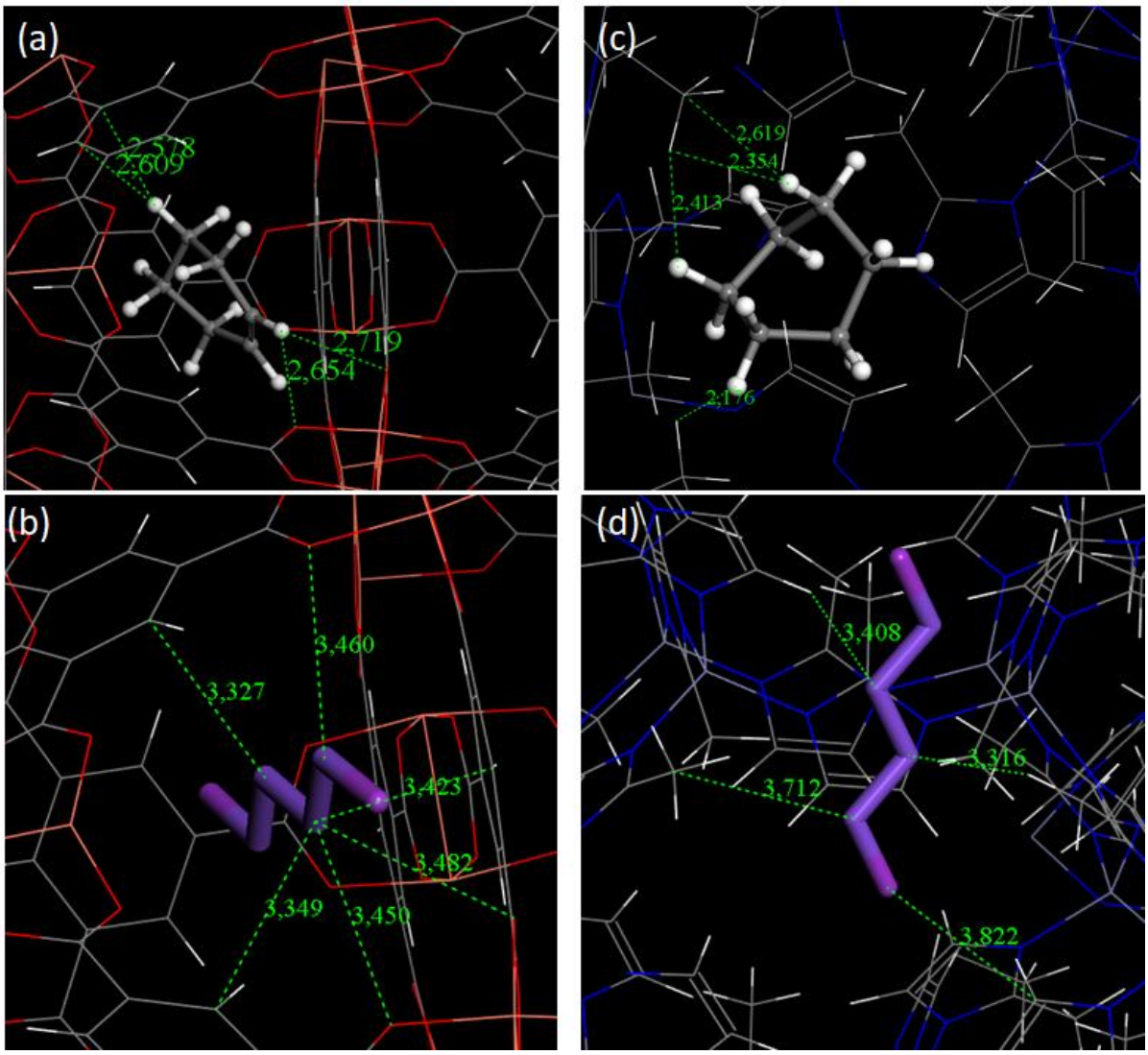

Figure 4. Snapshots for the main interactions between cyclohexene and n-hexane in Cu-BTC ((a) and (b) respectively) and in ZIF-8 ((c) and (d) respectively).

In the case of CoCo (Figure 5), stronger interactions are observed in the case of cyclohexene with unsaturated metal centers and with C≡N (2.8-3.0Å) than for *n*-hexane molecules (3.3-3.8Å). These are in good agreement with the adsorption enthalpies determined theoretically. It can be noticed that the *n*-hexane molecule interacts with the two sides of the pore, while cyclohexene, which is smaller in length, interacts with a more confined part of the pore.

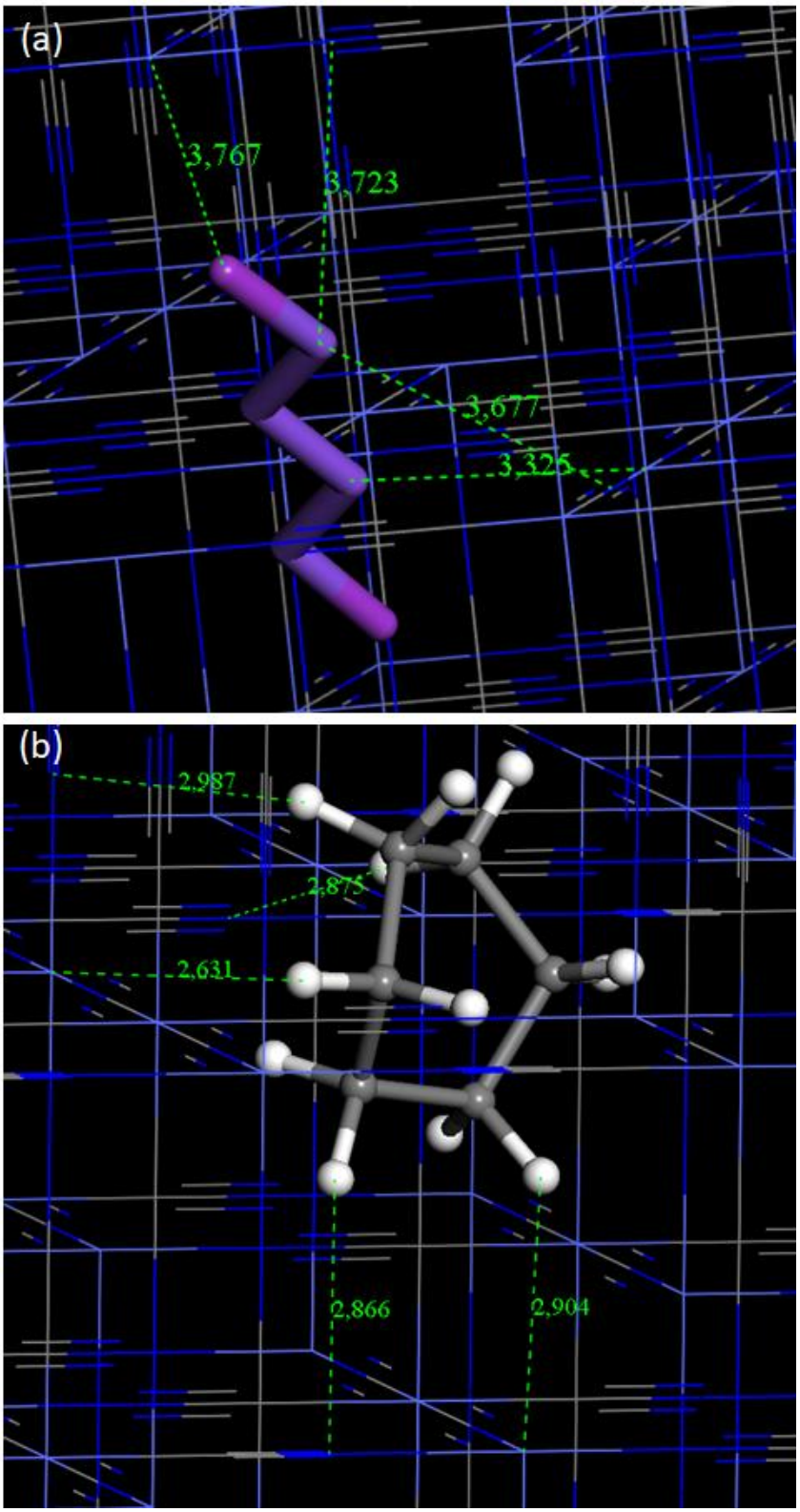

Figure 5. Snapshots for the main interactions between n-hexane (a) and cyclohexene (b) in CoCo.

3.3. Hydrostability.

The hydrostability of the investigated host frameworks was investigated after water adsorption by using PXRD and nitrogen adsorption isotherms. The PXRD patterns for the three materials performed before and after water adsorption are shown in Figure 6. In the case of Cu-BTC (Figure 6a), the obtained diffractograms are clearly different clearly indicating the modification of the structure during the water sorption and low hydrostability. In the case of ZIF-8 (Figure 6b), the peak positions and the relative intensities on the PXRD patterns are similar for materials before and after water sorption, suggesting that the structure is preserved after contact with water.

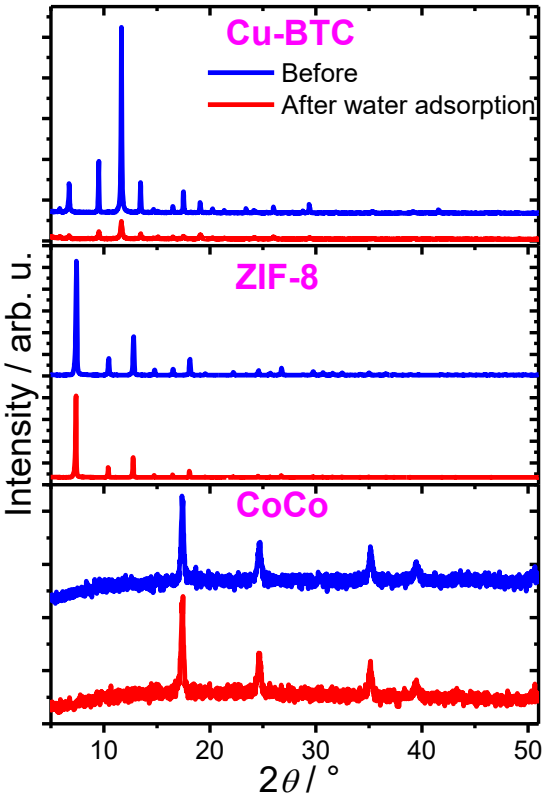

Figure 6. PXRD of Cu-BTC, ZIF-8 and CoCo.

Regarding CoCo (Figure 6c), both intensities, positions and relative intensities are preserved which is the indication that this material has a good hydrostability as already shown in the

past.[11] In order to complete this study, we evaluated the porosity of CoCo and ZIf-8 after water sorption and their reactivation by heating at 250°C for 8h (Figure 7). In the case of Cu-BTC, since the structure is disrupted, as shown by XRD, we did not perform such analysis.

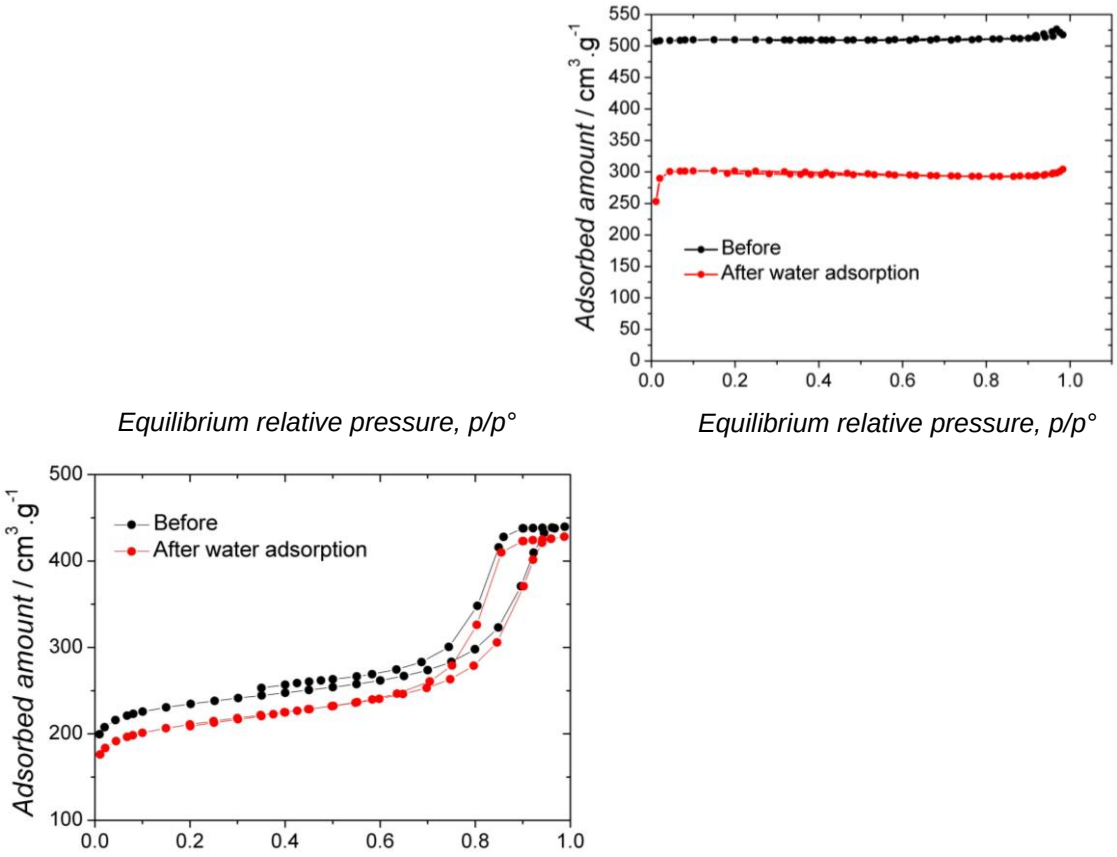

Figure 7. Nitrogen isotherm adsorption before and after water sorption. (left) ZIF-8; (right) CoCo.

The sorption isotherms obtained in the case of CoCo are clearly similar, before and after water adsorption. This confirms that the porosity is not impacted by the contact with water. Along with the XRD result, it can be deduced that CoCo has a high stability in water vapour atmosphere (Figure 7, right). In contrast, the nitrogen sorption isotherms obtained in the case of ZIF-8 (Figure 7, left) are different. The saturation plateau is lower (about one half lower for ZIF-8 after water sorption) and the affinity at low pressure is also decreased. This suggests

that the texture of ZIF-8 has been impacted by water sorption, despite the fact that it is hydrophobic. In contrast, the structure of ZIF-8 is preserved as the PXRD look similar before and after water exposure.

4. Conclusion.

In summary, we have compared here the performances for selected hydrocarbons sorption of a synthesised cobalt-based Prussian Blue Analogue with referenced commercial MOFs, such as ZIF-8 and Cu-BTC by using complementary experimental and theoretical approaches and propose the microscopic mechanisms occurring upon adsorption. While Cu-BTC is highly efficient for adsorption of the investigated hydrocarbons with large adsorption capacities (150 $mg.g^{-1}$), it has proven to be unstable in the presence of water and cannot be used for humid hydrocarbons adsorption and separation. In the case of the hydrophobic ZIF-8, *n*-hexane is preferentially adsorbed (250 $mg.g^{-1}$ at saturation), whereas cyclohexene is not, due to the size of the windows, which prevents the molecule from entering to the network's porosity. ZIF-8 is highly hydrophobic and does not adsorb water. Yet, even if its structure is preserved, its porosity decreases after water adsorption, which seems to be problematic for its use as adsorbent materials for humid hydrocarbons adsorption and separation. On the contrary, CoCo is stable in humid conditions and even if its sorption capacity is lower than that found for the other MOFs investigated, it seems more appropriate for humid hydrocarbons sorption or separation. Beyond the study of single components sorption in these materials, it would be of interest to focus on the sorption of mixed vapours including water. Indeed, water is often present in industrial applications (gas purification, separations etc).

Literature

[1] J. Magné-Drisch, Tech. l'ingénieur J5482 V1 (2016).

[2] Gas Process Suppliers Association Engineering Data Book, Edition 11, 2004.

[3] R.Q. Snurr, O.K. Farha, T. Islamoglu, J.T. Hupp, A.J. Howarth, M.L. Mendonca, N.S. Bobbitt, Chem. Soc. Rev. 46 (2017) 3357–3385.

[4] N. Soltys, Tech. l'ingénieur 33 (1998) 1–2.

[5] A. Rojey, E. Lebas, N. Doerler, J. Larue, Procédé de Déshydratation et de Dégazolinage d'un Gaz, Comportant Un Étage de Refroidissement Préliminaire, EP 0 835 921 A1, 1998.

[6] J.P. Bellat, J.C. Moise, V. Cottier, C. Paulin, A. Methivier, Sep. Sci. Technol. 33 (1998) 2335–2348.

[7] A. Zarate, R.A. Peralta, P.A. Bayliss, R. Howie, M. Sanchez-Serratos, P. Carmona-Monroy, D. Solis-Ibarra, E. Gonzalez-Zamora, I.A. Ibarra, RSC Adv. 6 (2016) 9978–9983.

[8] N.A. Travlou, E. Rodríguez-Castellón, T.J. Bandosz, Carbon N. Y. 100 (2016) 64–73.

[9] R. Glaser, J. Weitkamp, Handb. Porous Solids 1 (2002) 395–431.

[10] L.N. Ho, Y. Schuurman, D. Farrusseng, B. Coasne, J. Phys. Chem. C 119 (2015) 21547–21554.

[11] L. Boudjema, E. Mamontova, J. Long, J. Larionova, Y. Guari, P. Trens, Inorg. Chem. 56 (2017) 7598–7601.

[12] N.A. Ramsahye, T.K. Trung, S. Bourrelly, Q. Yang, T. Devic, G. Maurin, P. Horcajada, P.L. Llewellyn, P. Yot, C. Serre, Y. Filinchuk, F. Fajula, Ǵrard Ŕey, P. Trens, J. Phys. Chem. C 115 (2011) 18683–18695.

[13] P.A.P. Mendes, P. Horcajada, S. Rives, H. Ren, A.E. Rodrigues, T. Devic, E. Magnier, P. Trens, H. Jobic, J. Ollivier, G. Maurin, C. Serre, J.A.C. Silva, Adv. Funct. Mater. 24 (2014) 7666–7673.

[14] J.-R. Li, R.J. Kuppler, H.-C. Zhou, Chem. Soc. Rev. 38 (2009) 1477–504.

[15] A. Noureddine, P. Trens, G. Toquer, X. Cattoen, M. Wong Chi Man, Langmuir 30 (2014) 12297–12305.

[16] P.M. Schoenecker, C.G. Carson, H. Jasuja, C.J.J. Flemming, K.S. Walton, Ind. Eng.

Chem. Res. 51 (2012) 6513–6519.

[17] J. Duan, W. Jin, S. Kitagawa, Coord. Chem. Rev. 332 (2017) 48–74.

[18] T. Kajiwara, H. Higashimura, M. Higuchi, T. Yamada, H. Kitagawa, D. Watanabe, Chem. - A Eur. J. 20 (2014) 15611–15617.

[19] T.K. Trung, N.A. Ramsahye, P. Trens, N. Tanchoux, C. Serre, F. Fajula, G. Férey, Microporous Mesoporous Mater. 134 (2010) 134–140.

[20] P. Trens, H. Belarbi, C. Shepherd, P. Gonzalez, N.A. Ramsahye, U.H. Lee, Y.K. Seo, J.S. Chang, Microporous Mesoporous Mater. 183 (2014) 17–22.

[21] F. Karadas, H. El-Faki, E. Deniz, C.T. Yavuz, S. Aparicio, M. Atilhan, Microporous Mesoporous Mater. 162 (2012) 91–97.

[22] G. Férey, Chem. Soc. Rev. 37 (2008) 191–214.

[23] J. Canivet, A. Fateeva, Y. Guo, B. Coasne, D. Farrusseng, Chem. Soc. Rev. (2014) 5594–5617.

[24] A.U. Ortiz, A.P. Freitas, A. Boutin, A.H. Fuchs, F.-X. Coudert, Phys. Chem. Chem. Phys. 16 (2014) 9940–9949.

[25] L. Boudjema, J. Long, F. Salles, J. Larionova, Y. Guari, P. Trens, Chem. A Eur. J. 25 (2019) 479–484.

[26] P. Trens, N. Tanchoux, D. Maldonado, A. Galarneau, F. Di Renzo, F. Fajula, New J. Chem. 28 (2004) 874.

[27] P. Trens, N. Tanchoux, A. Galarneau, D. Brunel, B. Fubini, E. Garrone, F. Fajula, F. Di Renzo, Langmuir 21 (2005) 8560–8564.

[28] T. Düren, F. Millange, G. Férey, K.S. Walton, R.Q. Snurr, J. Phys. Chem. C 111 (2007) 15350–15356.

[29] A.K. Rappé, C.J. Casewit, K.S. Colwell, W.A. Goddard III, W.M. Skid, J. Am. Chem. Soc. 114 (1992) 10024–10035.

[30] L.D. Gelb, K.E. Gubbins, Langmuir 15 (1999) 305 6 308.

[31] P. Horcajada, H. Chevreau, D. Heurtaux, F. Benyettou, F. Salles, T. Devic, A. Garcia-Marquez, C. Yu, H. Lavrard, C.L. Dutson, E. Magnier, G. Maurin, E. Elkaïm, C. Serre, Chem. Commun. 50 (2014) 6872.

[32] V. Armel, S. Hindocha, F. Salles, S. Bennett, D. Jones, F. Jaouen, J. Am. Chem. Soc. 139 (2017) 453–464.

[33] D. Frenkel, B. Smit, Understanding Molecular Simulation From Algorithms to Applications, 2nd ed., 2002.

[34] A.K. Rappé, C.J. Casewit, K.S. Colwell, W.A. Goddard, W.M. Skiff, J. Am. Chem. Soc. 114 (1992) 10024–10035.

[35] J. Abascal, C. Vega, J. Chem. Phys. 123 (2005) 234505.

[36] M.G. Martin, J.I. Siepmann, J. Phys. Chem. B 102 (1998) 2569–2577.

[37] S.J. Keasler, S.M. Charan, C.D. Wick, I.G. Economou, J.I. Siepmann, J. Phys. Chem. B 116 (2012) 11234–11246.

[38] T. Devic, F. Salles, S. Bourrelly, B. Moulin, G. Maurin, P. Horcajada, C. Serre, A. Vimont, J.C. Lavalley, H. Leclerc, G. Clet, M. Daturi, P.L. Llewellyn, Y. Filinchuk, G. Férey, J. Mater. Chem 22 (2012) 10266–10273.

[39] F. Salles, G. Maurin, C. Serre, P.L. Llewellyn, J. Long, H. Choi, Y. Filinchuk, G. Férey, J. Am. Chem. Soc. 132 (2010) 13782–13788.

[40] J. Perdew, Y. Wang, Phys. Rev. B 45 (1992) 13244–13249.

[41] A. Phan, C.J. Doonan, F.J. Uribe-Romo, C.B. Knobler, M. O'Keefe, O.M. Yaghi, Acc. Chem. Res. 43 (2010) 58–67.

[42] S.S.Y. Chui, S.M.F. Lo, J.P.H. Charmant, A.G. Orpen, I.D. Williams, Science (80-.). 283 (1999) 1148–1150.

[43] A.P. Cote, J.Y. Choi, Z. Ni, R. Huang, H.K. Chae, K.S. Park, M. O'Keeffe, F.J. Uribe-Romo, O.M. Yaghi, Proc. Natl. Acad. Sci. 103 (2006) 10186–10191.

[44] T. Terencio, F. Di Renzo, D. Berthomieu, P. Trens, J. Phys. Chem. C 117 (2013) 26156–26165.

[45] J.P. Zhang, Y.B. Zhang, J. Bin Lin, X.M. Chen, Chem. Rev. 112 (2012) 1001–1033.

[46] J.B. James, Y.S. Lin, J. Phys. Chem. C 120 (2016) 14015–14026.

[47] S.S. Kaye, J.R. Long, J. Am. Chem. Soc. 127 (18), (2005) 6506–6507.

[48] S.S. Kaye, J.R. Long, Catal. Today 120 (2007) 311–316.

[49] L.E. Kreno, K. Leong, O.K. Farha, M. Allendorf, R.P. Van Duyne, J.T. Hupp, Chem. Rev. 112 (2012) 1105–25.

[50] G. Férey, Dalton Trans. (2009) 4400–15.

Graphical abstract

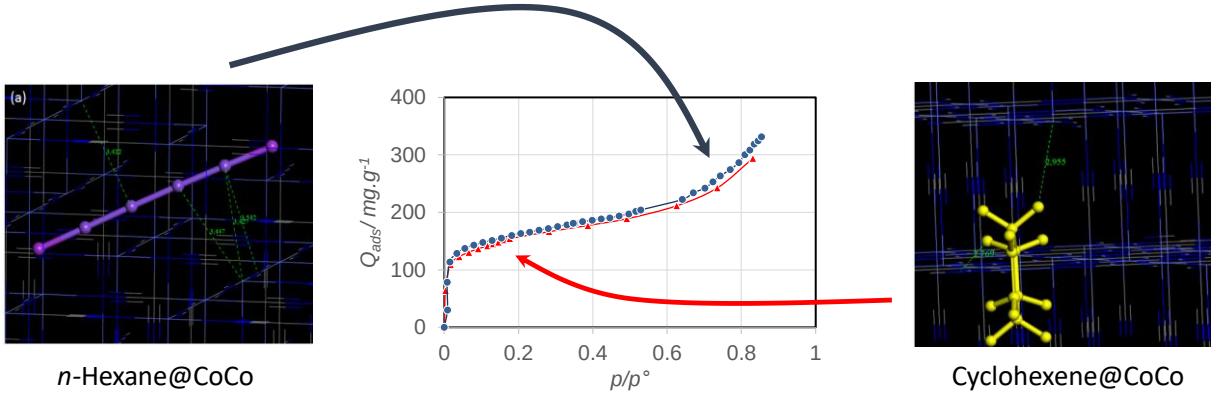

n-Hexane@CoCo

Cyclohexene@CoCo